J. Fluid Mech. (1988), *vol.* 189, *pp.* 135–163
Printed in Great Britain

Development of the turbulent near wake of a tapered thick flat plate

By A. HAJI-HAIDARI AND C. R. SMITH
Department of Mechanical Engineering and Mechanics, Lehigh University, Bethlehem, PA 18015, USA

(Received 14 August 1986 and in revised form 2 September 1987)

The velocity field and turbulence structure in the near wake of a thick flat plate with a tapered trailing-edge geometry are examined using both hydrogen-bubble flow visualization and hot-film anemometry measurements. Tests were conducted for $Re_1 = 8.5 \times 10^5$ in the region $0 < x^+ < 6400$ behind the trailing edge. The probe and visualization results indicate a similarity between both (i) velocity and turbulence structure variations wih x^+ in the near wake, and (ii) the corresponding changes in similar flow characteristics with y^+ within a turbulent boundary layer. In particular, visualization data in the vicinity of the wake centreline reveal the existence of strong streamwise flow structures in the region close ($x^+ < 270$) to the trailing edge. The streamwise orientation of the observed structures diminishes as x^+ increases. From hot-film measurements, two separate regions along the wake centreline can be distinguished: (i) a linear growth region which extends over $0 < x^+ < 100$, wherein the centreline velocity varies linearly with x^+; and (ii) a logarithmic growth region for $x^+ > 270$, wherein the centreline velocity varies as $\log x^+$. The similarity in behaviour between these regions and the comparable wall region of a turbulent boundary layer suggests the existence of a common functionality. This similarity is demonstrated by a simple linear relationship of the form $y^+ = Kx^+$, which is shown to approximately collapse the velocity behaviour both across a turbulent boundary layer and along the wake centreline to a unified set of empirical relationships.

1. Introduction

1.1. *Background*

The determination of the turbulent structure of the near wake generated by a streamlined body in a uniform stream, although important, has not received as much attention as the flow far downstream of the body. An understanding of the complicated flow characteristics which occur immediately behind an airfoil or a turbine blade has significant importance both in turbomachinery applications as well as for the aircraft industry. A knowledge of the flow behaviour in the vicinity of tapered trailing edges and the effects of the new boundary conditions on the flow field become of great interest for design purposes.

The wake flow behind a thin flat plate, the simplest form of turbulent near wake for a streamlined body, has received detailed study for the past two decades. A commonly referenced experimental study of this flow is that by Chevray & Kovasznay (1969), which was done in wind tunnel utilizing a single-element, slanted hot-wire anemometer which is rotated slowly through an angle of $\pm 80°$. The results suggest that: (i) no detectable periodicity was present in the wake, (ii) the wake develops very slowly, and (iii) the fluctuating components of velocity reach their

maximum value in the region of maximum shear stress. The momentum thickness at the trailing edge was used as a relative scale to non-dimensionalize the data.

Andreopoulos & Bradshaw (1980), in one of the most complete studies of the near wake flow of a flat plate, made detailed measurements of mean and fluctuating velocity components, double, triple and quadruple products of Reynolds stresses, and temperature intermittency at various stations in the symmetric and asymmetric wake. Using a heat contaminant, Andreopoulos & Bradshaw show that the outer portion of the wake is virtually unaffected by the disappearance of the trailing edge, except within the inner-wake region. They also suggest that the inner part of the near wake should scale on wall-layer parameters. The friction velocity u_τ and a wall-layer scaling approach were used to establish a logarithmic fit for the centreline velocity. A three-layer model for the wake flow immediately behind the plate was suggested (i.e. a layer of mixed fluid sandwiched between two layers of unmixed fluid). Andreopoulos & Bradshaw conclude that the initial boundary layer is unchanged as the flow leaves the plate, with significant changes in the unmixed fluid confined to the intermittent region, that is, between the boundaries of the 'mixed' and 'unmixed' fluid.

In another extensive investigation, Ramaprian, Patel & Sastry (1982) made detailed measurements of the mean flow of the 'developing' wake of a streamlined body. Their work suggests that the wake of a sharp trailing edge develops in three stages. First, a near wake $0 < x/\theta_1 < 25$ (θ_1 = momentum thickness of far wake) in which the centreline velocity distribution behaves as $x^{\frac{1}{3}}$. Second, an 'intermediate' logarithmic-type growth region, $25 < x/\theta_1 < 350$. Third, a region $x/\theta_1 > 350$, called an asymptotic wake, which behaves as a classical far wake.

1.2. *Overview*

The experimental studies discussed above cover only the primary studies for wake flow behind a flat plate. A detailed review of the experimental work is presented by Ramaprian *et al.* (1982). Additional information including a review of analytical investigations is well documented by Bogucz & Walker (1988).

A careful evaluation of all available experimental data provides the following general picture of the turbulent near wake. The data are consistent for a symmetric flat plate with a sharp trailing edge, indicating that the inner wake develops rapidly, while the logarithmic region of the boundary layer evolves slowly to a wake-like flow over 30 initial momentum thicknesses downstream. Momentum is conserved in the wake, since the pressure is constant in the x-direction; generally, there is a decrease in the shape factor just following separation, followed by an increase to a self-preserving limit about 300 initial momentum thicknesses downstream. Information that is lacking or incomplete is: (i) an appropriate lengthscale for the near wake, (ii) a consistent means of defining the inner and outer wake, (iii) the degree of periodicity in the wake, and (iv) the effect of the viscous sublayer on the wake behaviour immediately downstream of the trailing edge.

1.3. *Present study*

Presently, there appears to be very little visualization data for flows in the near wake of a flat plate. Visualization techniques normally provide only qualitative data, but such data are essential for proper interpretation of probe results. Visualization techniques also facilitate the overall investigation of the entire flow field, including regions where the flow separates or recirculates. Since visual data cannot generally

be used to effectively determine the quantitative flow characteristics, an alternative flow measurement technique is required to complement the visualization results.

The present study investigates the flow behaviour in the near wake of a thick flat plate with a tapered trailing edge. A thick plate provides a more realistic simulation of practical aerodynamic geometries than the thin plates used in most of the previous studies. In particular, the present geometry and flow conditions are configured to yield a boundary layer-to-plate thickness ratio of approximately one-half at the point of taper initiation, and a plate Reynolds number comparable with that experienced by a turbine-blade-type geometry.

The hydrogen-bubble technique is used to visualize the development and mixing of the separated turbulent boundary layer for approximately ten boundary-layer thicknesses downstream of the plate. Moreover, hot-film anemometry is used to determine the mean velocity and turbulence intensity profiles at various locations in the near wake to allow improved understanding and interpretation of the visualization data, and vice versa.

Briefly, the research objectives of the present study are to: (i) establish a more general understanding of the physics, dominant scales and mixing process(es) in the turbulent near wake of a thick flat plate with a tapered trailing edge; (ii) provide detailed visualization data to effectively illustrate the process of evolution of the flow structure from a flat-plate boundary layer to a near wake; (iii) compare and contrast the obtained results with previous investigations of near wake flow behind thin flat plates.

2. Experimental arrangement

The experiments were conducted in the Lehigh University free-surface Plexiglas water channel with a working section 5 m long, 0.9 m wide and 0.3 m deep. A detailed description of the flow facility and its characteristics is presented in Smith & Metzler (1983). The test model employed in the study (figure 1) was 10 cm thick, 30 cm wide and 288 cm in length and constructed of Plexiglas to allow appropriate lighting for hydrogen-bubble-visualization studies. The leading edge of the test model was a 5:1 half-ellipse. The trailing edge was tapered at 8° to 0.79 mm trailing-edge thickness. The junction corners, where the trailing-edge taper initiates, were rounded to avoid possible flow-separation effects; dye-injection studies confirmed flow attachment. The test model was mounted with its span in the vertical direction and was anchored with overhead support rods. All joints were filled with paraffin wax and faired to ensure flatness and to eliminate any cavity effects. Further details of the test model fabrication can be found in Haji-Haidari & Smith (1984).

Visualization studies of the trailing-edge-flow behaviour were done using hydrogen-bubble visualization and a high-speed video system (see Smith & Metzler 1983). 25 μm diameter platinum wire mounted in two *u*-shaped probes (see Haji-Haidari & Smith 1984) was used to generate hydrogen-bubble time lines in both vertical and horizontal planes. In the present work, time-line frequencies of 60 and 120 Hz were used. The hydrogen-bubble probes were mounted in a support mechanism which rides on an overhead traverse platform (Smith & Metzler 1983), such that time lines could be easily introduced anywhere in the channel.

Flow measurements were taken with a DISA-type 55M01 hot-film anemometer. Mean and fluctuating velocity were measured in the streamwise direction using a DISA 55R11 or 55R15 quartz hot-film probe mounted with the sensor parallel to the test-section walls. Owing to the low flow velocity employed (29 cm/s), the averaging

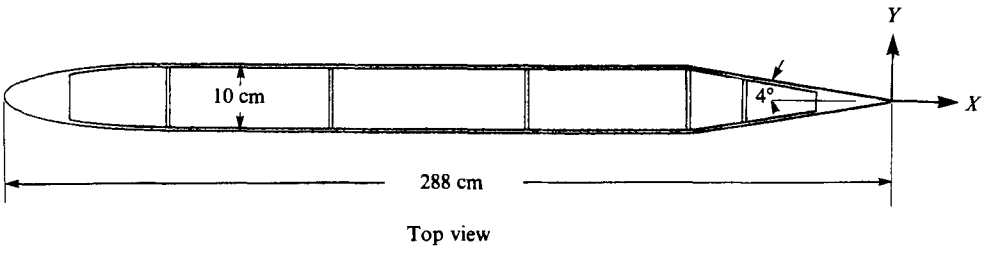

FIGURE 1. Schematic representation of the test plate.

time for each measurement point was 400 s, which ensured stable velocity readout using either a TSI-1076 digital voltmeter or a DEC PDP 11/23 computer data acquisition system. Each velocity and turbulence-intensity profile included sufficient points such that adjacent measurement points varied by no more than 10% of the maximum profile value.

3. Hot-film anemometry measurements

To ensure the presence of a fully developed turbulent boundary layer, mean-velocity profiles were measured on both sides of the test plate, 10 cm upstream of the trailing edge at $X = -2.0$ ($X = x/t$, $Y = y/t$: t = plate half-thickness prior to taper; see figure 1). As figure 2 shows, the shape of these profiles is not as 'full' as those of a typical flat-plate profile. This difference is due to the pressure gradient generated by the trailing-edge taper. Numerical integration of the boundary-layer profile yielded a shape factor of $H = \delta^*/\theta = 1.60$, which is higher than conventional flat-plate values, but commensurate with typical values for turbulent boundary layers subjected to a mild adverse pressure gradient. Within the range of uncertainty of the experimental data, the two velocity profiles appear reasonably symmetric.

Mean-wake-velocity profiles obtained at six downstream locations are shown in figure 3. Owing to channel length constraints, the last station at which profile measurements could be effectively made was $X = 12$ (60 cm downstream of the trailing edge), corresponding to 73 momentum thicknesses. One of the more striking aspects of these profiles is how little the wake spreads. For measurements to $X = 12$, the bulk of the defect region of the velocity profiles is contained between $Y = \pm 1.5$, which are essentially the edges of the intial flat-plate boundary layers. As can be observed, the changes in the velocity profiles are primarily confined to the inner wake. This is clearly illustrated in figure 4, with the data plotted in law-of-the-wall parameters. The normalizing friction velocity u_τ is established at $X = -2$ upstream of the trailing edge, using a numerical optimization technique outlined in Yuhas & Walker (1982).

Another important point that can be concluded from figure 4 is that growth of the inner region occurs from the centreline outward with increasing x, with limited modification of the outer region until the centreline growth effects encroach upon the logarithmic region. Figure 4 indicates a rapid recovery of the defect velocity in the inner-wake region for $X \leqslant 1$. The growth becomes more moderate for $X > 1$, with the mean-velocity profiles displaying limited growth from $X = 4$ to $X = 12$.

Turbulence intensity profiles were measured at six locations downstream of the trailing edge and are plotted in wall parameters as shown in figure 5. At the first downstream location ($X = 0$), the turbulence-intensity measurements are essentially the same as the typical turbulent-boundary-layer profiles measured on the plate at

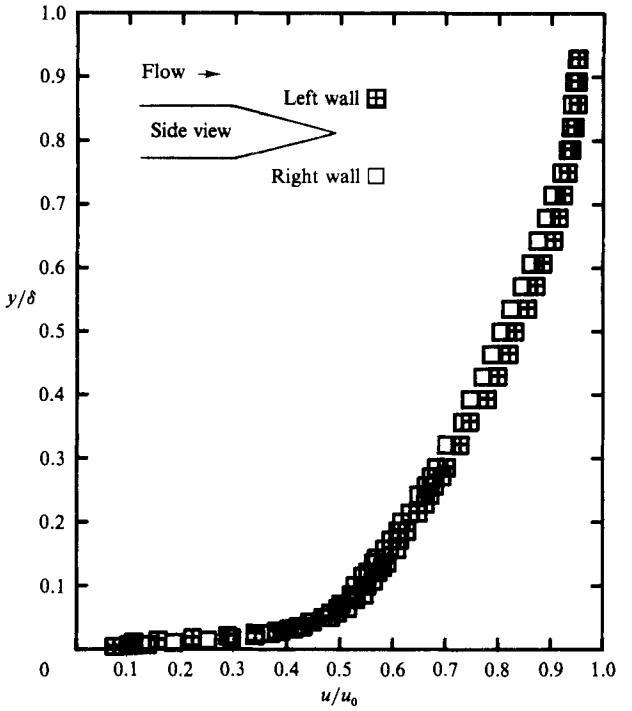

FIGURE 2. Boundary-layer profile at $X = -2.0$ from the trailing edge. $Re_1 = 8.50 \times 10^5$, $Re_\theta = 2.5 \times 10^3$.

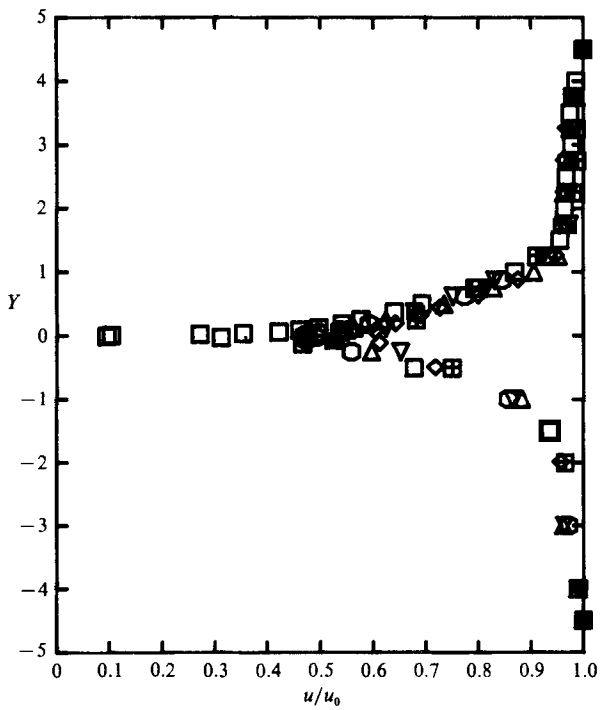

FIGURE 3. Wake mean-velocity profiles. □, $X = 0$; ○, 1.0; △, 2.0; ◇, 4.0; ▽, 8.0; ⊞, 12.0.

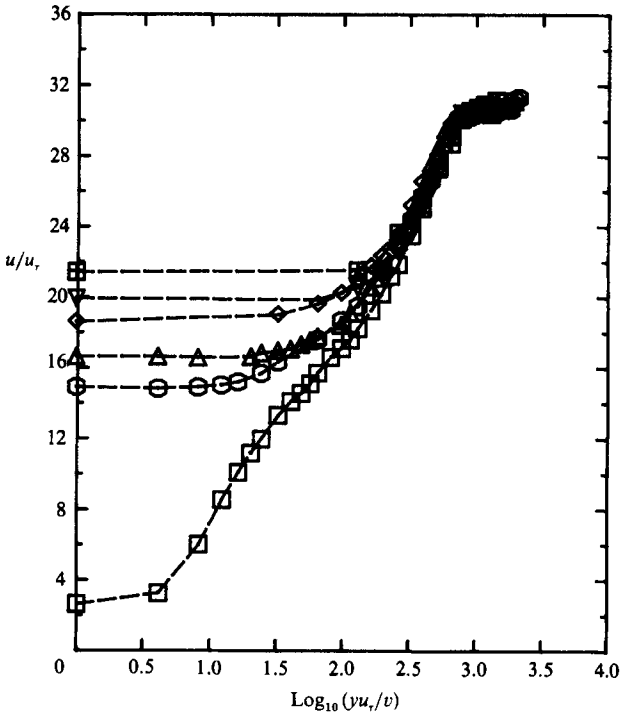

FIGURE 4. Wake mean-velocity profiles plotted in wall parameters. □, $X = 0$; ⬡, 1.0; △, 2.0; ◇, 4.0; ▽, 8.0; ⊞, 12.0.

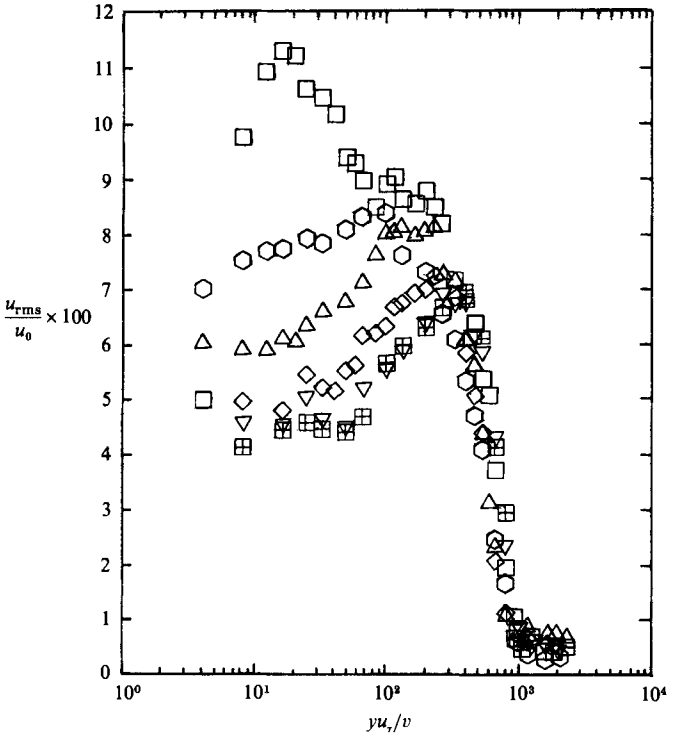

FIGURE 5. Wake turbulence-intensity profiles plotted in wall parameters. □, $X = 0$; ⬡, 1.0; △, 2.0; ◇, 4.0; ▽, 8.0; ⊞, 12.0.

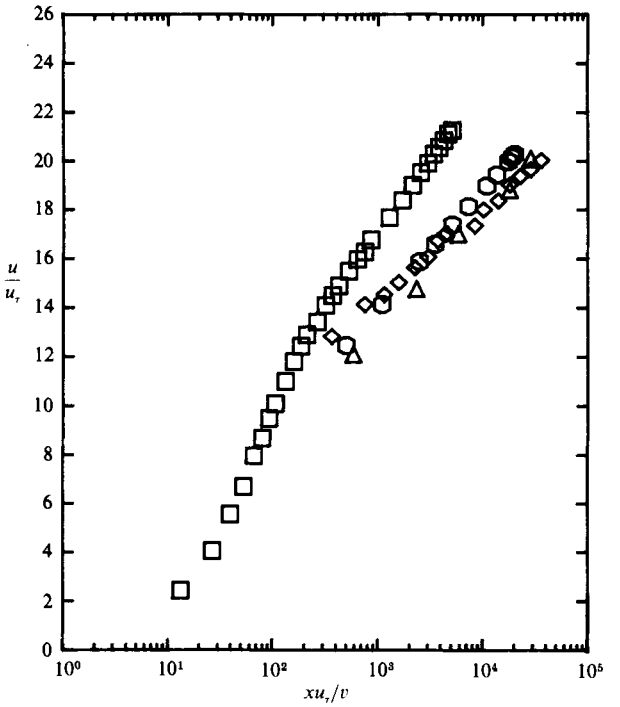

FIGURE 6. Centreline velocity: ○, Andreopoulos & Bradshaw (1980), $Re_\theta = 13.6 \times 10^3$; ◇, Ramaprian *et al.* (1982). $Re_\theta = 2.4 \times 10^3$; △, Chevray & Kovasznay (1969), $Re_\theta = 1.58 \times 10^3$; □, present, $Re_\theta = 2.5 \times 10^3$.

$X = -2$. A maximum intensity of 11.3% (relative to free-stream velocity) is measured at $X = 0$. This peak value reduces to 8.4% by $X = 1.0$; thereafter, the decrease is more moderate, with the maximum turbulence intensity reduced to 6.6% by the last streamwise location, $X = 12$. Two points should be noted. First, the point of maximum intensity continuously migrates away from the centreline. For example, at $X = 1.0$ the peak intensity occurs at $y^+ \approx 160$, at $X = 12$ the peak has shifted to $y^+ \approx 400$. Second, there is essentially no growth of the turbulence-intensity profiles beyond the limits of the original boundary layer (i.e. $y^+ \approx 800$). The same limitation on the spreading of wake characteristics was previously observed for the mean-velocity profiles (figure 3). The intensity results are a further indication of the confined spreading of the wake.

Figure 6 is a plot of centreline velocity as a function of streamwise distance (in wall coordinates) which illustrates the development of logarithmic behaviour for $x^+ > 300$ ($x^+ = xu_\tau/\nu$). Below $x^+ = 300$, the centreline velocity departs from the logarithmic behaviour and asymptotically approaches zero in a fashion very similar to the velocity behaviour observed in the sublayer of a turbulent boundary layer. For $100 < x^+ < 300$, the velocity passes through a buffer-layer-like region which provides transition from linear to logarithmic behaviour. To emphasize the logarithmic behaviour of the velocity on the centreline, the experimental data of Chevray & Kovasznay (1969), Andreopoulos & Bradshaw (1980) and Ramaprian *et al.* (1982) are shown for comparison. The starting point for logarithmic growth of the centreline velocity is almost the same for all cases shown; however, the slope of the curves is not. One of the reasons for this discrepancy is the difference in the values of the

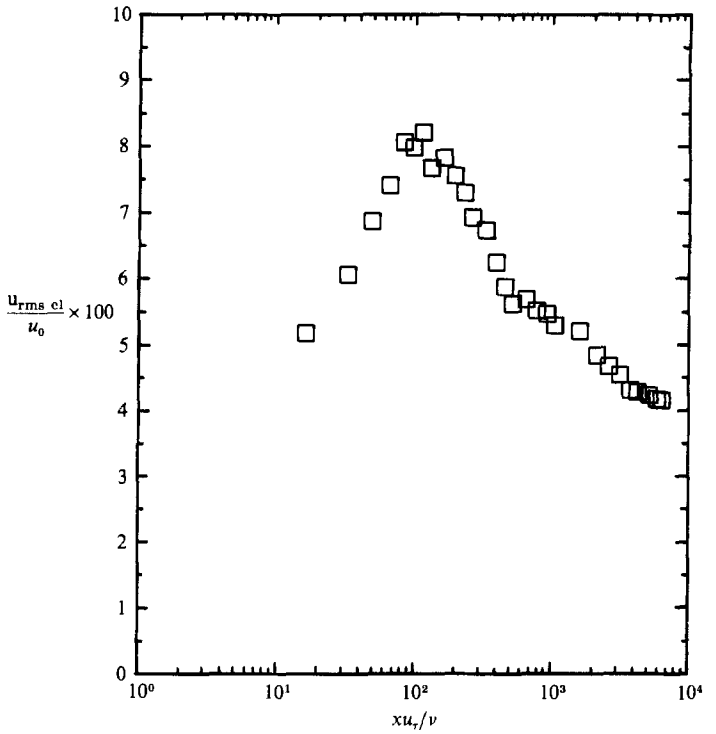

FIGURE 7. Wake centreline turbulence-intensity profile.

normalizing friction velocity u_τ. In the present study the plate was quite thick, creating an extended adverse pressure gradient over the tapered trailing edge, which was not present for the other three investigations shown. This adverse pressure gradient in front of the trailing edge results in a lower value of u_τ, and a higher value of u_0/u_τ. Despite the differences between the four sets of data shown in figure 6, it is clear that the centreline velocity grows logarithmically for $x^+ > 300$. The present studies could only be carried out to $x^+ = 6400$, but from previous investigations (e.g. Andreopoulos & Bradshaw, Ramaprian *et al.*) it appears that the logarithmic behaviour of the centreline velocity extends at least to $x^+ = 10^5$. Further discussion of the logarithmic behaviour of the centreline velocity appears in §5.2.

The corresponding plot of centreline turbulence intensity as a function of streamwise distance is shown in figure 7. Interestingly, the variation of turbulence intensity with increasing x is remarkably similar to the variation of the turbulence intensity within a turbulent boundary layer with increasing distance from the wall. In both cases, a rapid, almost linear increase is observed which quickly reaches a peak, followed by a much slower decrease with further departure from the origin. An additional aspect of this similarity is that in both cases the development of a peak in turbulence intensity is essentially commensurate with the initiation of a logarithmic variation of the mean velocity (cf. figures 6 and 7).

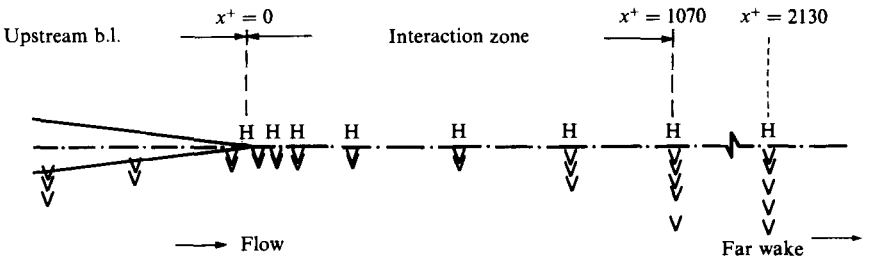

FIGURE 8. Streamwise location of the hydrogen-bubble probes. V, vertical (plane view); H, horizontal (side view).

4. Visualization studies

Figure 8 illustrates the streamwise locations visualized with the corresponding bubble-wire configurations. The plan-view studies examined the flow behaviour in the region $-1.25 < X < 4.0$, and $0 < Y < 1.0$, whereas side-view visualizations were obtained in the region $0 < X < 4.0$, and $-2.0 < Y < 2.0$. The horizontal hydrogen-bubble wire was employed for side-view visualizations, and the vertical bubble wire for plan-view. The downstream interval between two subsequent probe placements was selected depending upon how drastically the flow characteristics changed from one location to the next. Throughout this paper, whenever a visualization picture or sequences of pictures are shown, the wire location relative to the trailing edge is specified.

Overall, almost two hours of visualization data were recorded. Naturally, there is a limit to the number of pictures that can be presented while still enabling the reader to understand the very complicated flow behaviour existing in the wake. Furthermore, stop-action pictures do not effectively transmit the complexities of the dynamic behaviour which are apparent in the real-time and slow-motion video playback. Thus, schematic representations are presented in conjunction with individual pictures or series of pictures to emphasize the important characteristics illustrated in the visualizations.

4.1. *Plan-view studies*

The existence of an ordered structure, within the near-wall region of turbulent boundary layers, known as low-speed streaks, is well established. Numerous qualitative and quantitative studies of turbulent flow over a flat surface (e.g. Kline *et al.* 1967; Smith & Metzler 1983) have reported detection or observation of the coherent streamwise regions which characterize the low-speed streaks. In the present study, similar streak structures were observed in certain regions of the wake as well as on the test plate, which indicates the persistence of the organized spanwise structure.

Figure 9, is a plan-view, stop-action video picture with the bubble wire located over the test model upstream from the trailing edge ($X = -1.25$, $y^+ = (yu_\tau/\nu) \approx 10$). The bright streamwise concentrations of bubbles are the low-speed streaks which extend longitudinally near the wall, and migrate back and forth transversely across the wall. A study by Kline *et al.* (1967) suggests that the major production of the turbulent energy (up to 80%) in the inner region of the boundary layer is the result of the 'bursting' of these low-speed streaks from the near-wall regions. Kline *et al.* hypothesized that the 'bursting' is the primary means by which turbulent kinetic energy is transported to the outer or wake region of the boundary layer. The low-

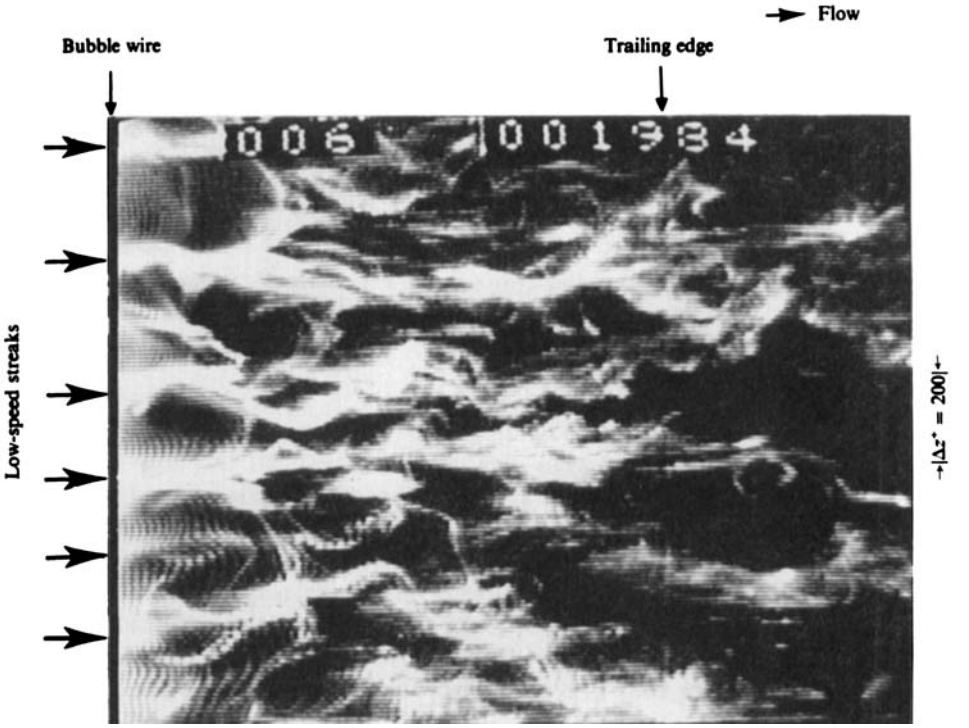

FIGURE 9. Plan view showing low-speed streaks over the test plate. $X_{\text{wire}} = -1.25$, $y^+ = 10$, $F_{\text{HB}} = 120$ Hz.

speed streaks are also believed (Smith 1984) to be the most universally organized and identifiable structure within the entire boundary layer.

Figure 9 clearly illustrates that the spacing between adjacent streaks is not consistent. A general description of the spacing between the low-speed regions is commonly done via statistical evaluation of the mean transverse streak spacing. One of the more detailed studies on low-speed streak characteristics was done by Smith & Metzler (1983), wherein they describe a technique for establishing streak spacing. The same technique was employed in the present study. The streak counting technique applied to the flat-plate data resulted in $\bar{\lambda}^+ = 100 \pm 15$. This value is essentially identical with those of previous investigations by Kline *et al.* (1967) and Smith & Metzler (1983).

Longitudinally dominant structures which retain the essential characteristics of low-speed streaks were observed in the wake as far as $x^+ = 130$ downstream of the trailing tip. This observation suggests that the low-speed streak organization in the near-wall boundary layer is not immediately affected by the disappearance of the wall, and persists into the immediate near-wake region. Visualization of the low-speed streak-type regions was done at two different normal heights, $y^+ < 5$ and $y^+ \approx 10$, and $x^+ = -600$, -30 on the test-model wall, and $x^+ = 30$, 70 and 130 in the wake ($x^+ = xu_\tau/\nu$). Figure 10(*a*, *b*) illustrates a distinct similarity between the flow pattern observed at a location $x^+ = -600$ (upstream of the model trailing edge, figure 10*a*), and at $x^+ = 130$ (downstream of the tip, figure 10*b*). The corresponding probability histograms established at each location from detailed streak-spacing measurements are also presented. The two histograms are similar in mean and standard deviations; however, differences in skewness and flatness are apparent. In

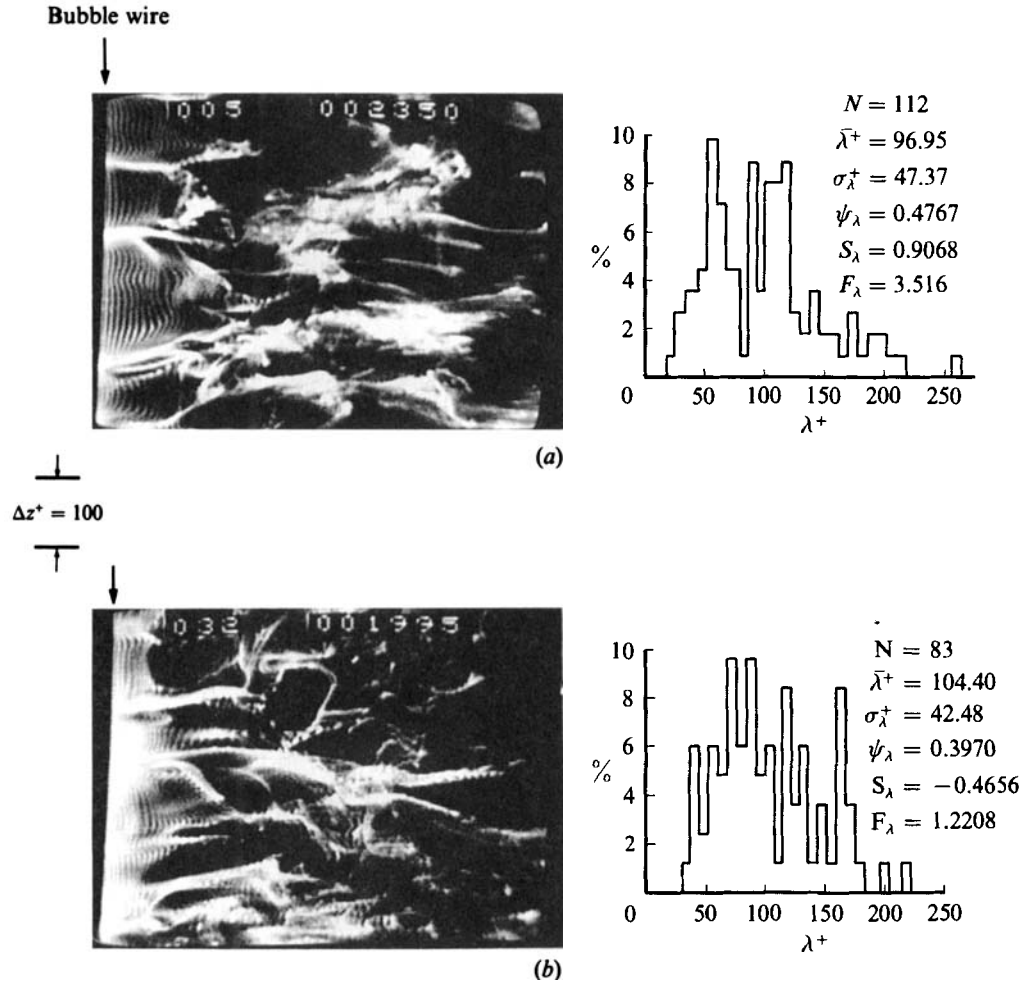

FIGURE 10. Plan-view visualization of low-speed streaks accompanied by streak-spacing histograms. (*a*) Flow over the test plate, $x^+_{\text{wire}} = -600$, $y^+_{\text{wire}} \approx 10$; (*b*) wake flow, $x^+_{\text{wire}} = 130$, $y^+_{\text{wire}} \approx 10$ (same magnification).

general, figure 10 indicates that the low-speed structures appear to have the same essential characteristics in the wake as they do above the test plate. In the wake, the streak count technique indicated little variation in streak spacing with streamwise distance, with $\bar{\lambda}^+ \approx 100 \pm 20$, which is in agreement with the flat-plate data. The histograms of the streak spacing indicated: (i) a slight increase in the mean streak spacing in the wake as y increased, (ii) a broadening of the streak distribution as distance from the wall (or the centreline) increased, and (iii) a broadening with increased x. Details of these measurements can be found in Haji-Haidari & Smith (1984).

Figure 11 is a series of four plan-view pictures, obtained with the bubble wire on the wake centreline at four different streamwise locations (location uncertainty $y^+ = \pm 2$). This figure illustrates the flow structure along the wake centreline and its modification with distance from the trailing edge. Close to the tip ($x^+ < 130$), the

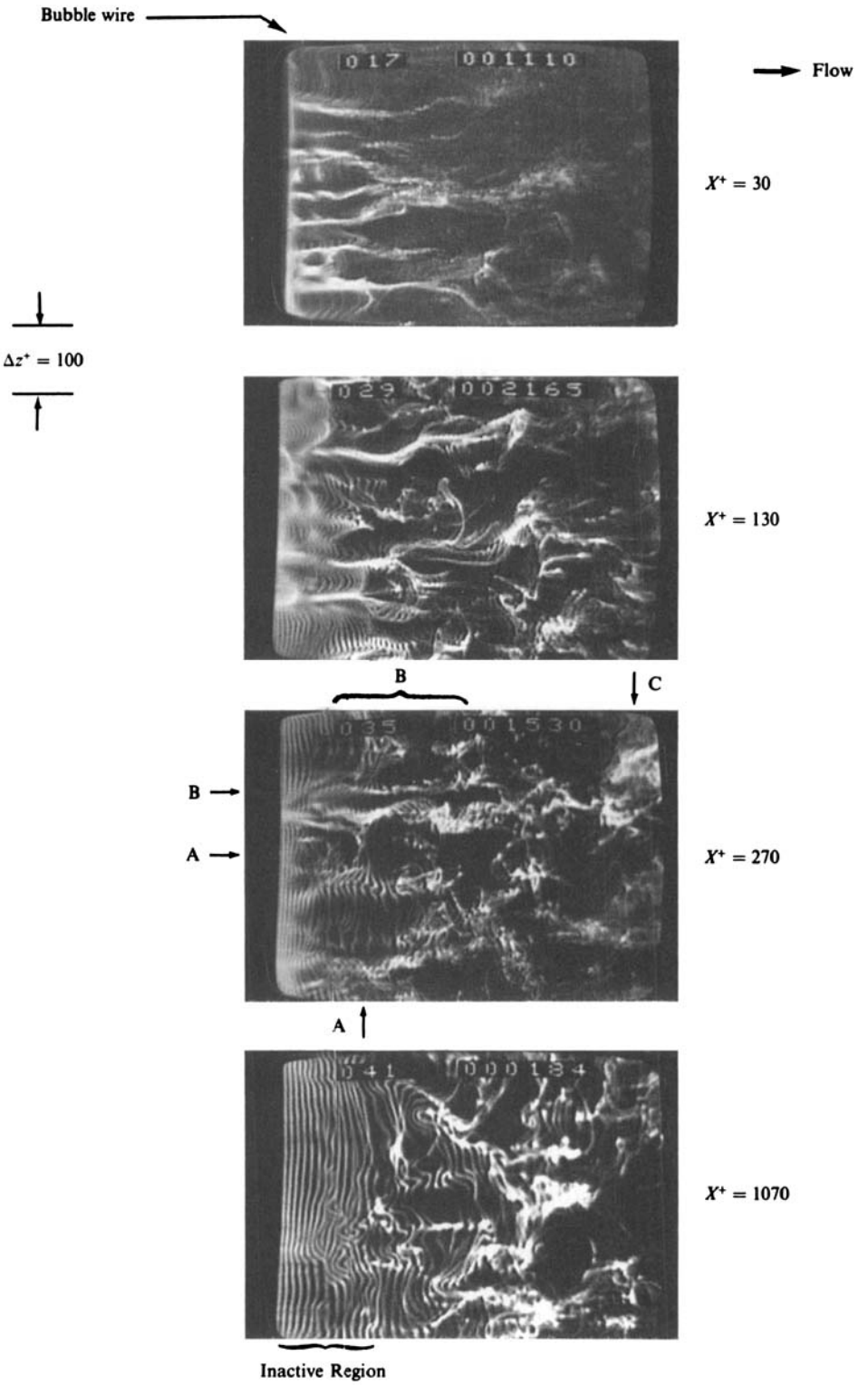

FIGURE 11. Variation of scale and flow-structure characteristics along wake centreline.

disturbances are more organized and coherent, with the bubble-line markers illustrating a dominant streamwise low-speed streak-type behaviour. Flow in this region retains scales comparable with those detected in the near-wall region of the turbulent boundary layer on the test model. Note that for $x^+ = 130$, the streamwise structures 'kink' much more than for $x^+ = 30$. At $x^+ = 270$, the disturbances appear less coherent, with a subsequent reduction in the observed streamwise organization. Owing to the modification of the streamwise structures, beyond $x^+ = 130$ the streaks were in general not sufficiently well defined, and a streak count consistent with the criteria used for previous visualization data was not applicable. However, from the visualization data, it was qualitatively observed that the transverse scale of the disturbances appears to increase with x.

Although not truly homogeneous, by $x^+ = 1070$ the disturbances have essentially lost a directional preference. Noting that the deformation of the bubble lines is caused only by 'active' local flow structure, the presence of a large 'inactive region' at $x^+ = 1070$ becomes apparent just downstream of the bubble wire; the presence of such an 'inactive' region is typical of the bubble-line patterns at this streamwise location. Comparison of the four pictures in figure 11 indicates that the lengthscale of transverse disturbances increases with increasing distance from the tip. Qualitative estimates suggest that the typical lengthscale at $x^+ = 1070$ has increased to approximately $l^+ = 150$ ($l^+ = lu_\tau/\nu$). Note that a corresponding increase in length scale with increasing distance from the boundary surface is also observed for turbulent boundary layers. For example, the results of Smith & Metzler (1983) and Nakagawa & Nezu (1981) indicate that lengthscales increase almost linearly with distance from the surface.

Figure 12 is shown to further illustrate the similarity between wake and turbulent-boundary-layer flow structure. In the two visualization pictures shown in figure 12 (obtained with identical magnification) the bubble wire was located above the test model at $y^+ = 130$ for figure 12(*a*), and downstream in the wake at $x^+ = 1070$ and $y^+ = 270$ (away from the centreline) for figure 12(*b*). It is clear from these pictures (which are truly representative for both cases) that in the regions removed from the wall and the wake centreline, the flow structure of a turbulent boundary layer and the downstream wake are markedly similar. It appears from these comparative pictures that there is neither a direction in which the disturbances are clearly dominant, nor a behaviour that can be singled out as most important. Therefore, it certainly appears that the scales in the outer portion of the boundary layer undergo little substantive change upon passage into the outer region of the near wake; this is also borne out by the narrowness of the wake interaction region within the near wake, as shown previously in §3.

4.2. *Side-view horizontal bubble wire*

Side-view visualizations are generally the most effective view for observation of (i) the mixing of the two merging boundary layers, (ii) the overall modification of the boundary-layer structure, and (iii) the wake growth. The visualization data allow the boundary of the mixed and unmixed regions for $x^+ < 270$ to be clearly identified; the mixing boundary is not clearly identifiable for $x^+ > 270$. To facilitate a common terminology, the region of intense vortex interactions is considered as the mixed region. The portion of the upstream turbulent boundary layer not affected by the mixing region is termed the unmixed wake.

In general, three distinguishable regions can be identified: (i) $0 < x^+ < 15$, where

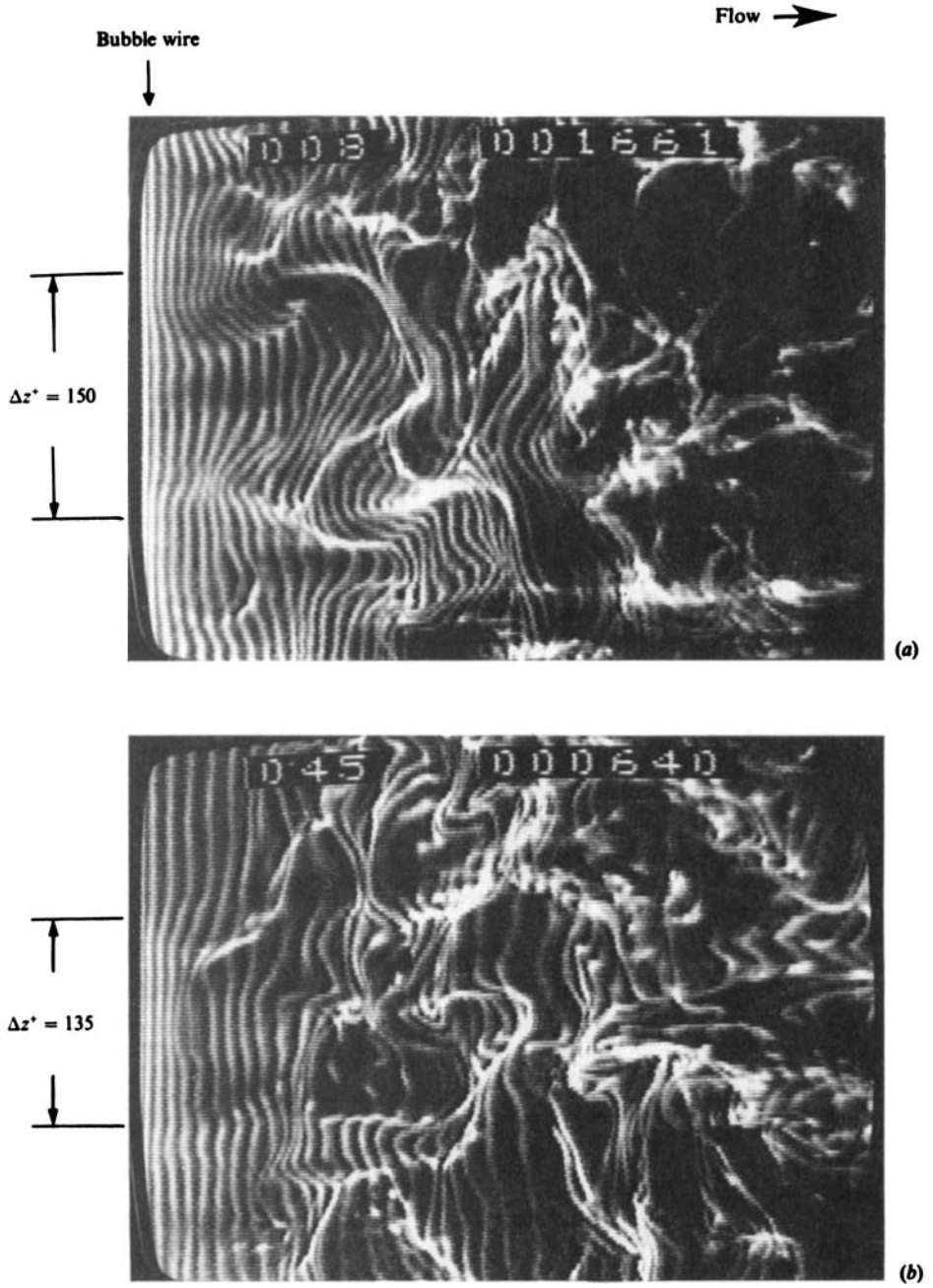

FIGURE 12. Similarity in scales of turbulence structures in the logarithmic region of the boundary layer upstream and downstream of the trailing edge. (*a*) $y^+_{\text{wire}} = 130$, $x^+_{\text{wire}} = -600$; (*b*) $y^+_{\text{wire}} = 270$, $x^+_{\text{wire}} = 1070$ (same magnification).

a small unsteady bubble of stagnant flow is formed owing to the finite thickness of the tip of the trailing edge; (ii) $15 < x^+ < 270$, which is a region of strong inward flow with the mixing process confined to the small-scale structures; (iii) $x^+ > 270$, where interaction occurs between groups of larger eddies of similar lengthscale. Further results on the mixing processes are presented in the following two sub-sections.

4.2.1. *Mixing in the region* $0 < x^+ < 270$

The visualization data indicate that the most intense flow interactions occur in the region $0 < x^+ < 270$. The discussion in §4.1 dealt with the rapid increase in centreline velocity in this region, as well as the merging of the boundary layers. Flow in this zone is also affected by the tip thickness and viscous-sublayer interaction. Locating the hydrogen-bubble wire at $X = 0$ revealed some interesting and complicated behaviour in this region. Figure 13 (*a*, *b*) is two pictures from the same video sequence (7.2 s apart) which show typical modes of interaction between the two merging boundary layers. Figure 13 (*a*) suggests that the two boundary layers merge and mix in a relatively narrow region. However, figure 13 (*b*) illustrates a broader region of shear-layer merging. The dynamic sequence, from which this picture was taken, reveals the presence of an inrush of fluid from both sides of the plate towards the centreline immediately downstream of the trailing edge. From a detailed review of the dynamic sequence it appears that the fronts of inward-moving fluid develop regions of strong streamwise vorticity, which appear to concentrate into streamwise vortices that are subsequently stretched in the streamwise direction. Figure 13 (*b*) further illustrates the following features of the wake mixing process: (i) a bright, narrow wavy region at the centreline which is the slow-moving trace left behind from the interaction between previous fronts, such as the behaviour shown in figure 13 (*a*); (ii) inward-moving fronts in the boundary layer (bright inclined regions) which form on both sides of the plate; and (iii) an apparent streamwise rotation appearing in the upper portion of the figure and extending $\Delta x^+ = 460$ downstream of the trailing edge.

Figure 13 (*c*) is a schematic that attempts to clarify the dominant mixing processes in this near-wake region. This schematic, a synthesized picture of the types of characteristic motions and mixing behaviour, was developed after review of numerous video sequences obtained with the bubble wire at or near the trailing edge. In order to properly interpret figure 13 (*c*), one should note the following: (i) the solid lines selectively illustrate the appearance of the bubble lines; (ii) the dashed lines define the fronts of regions of inflow; and (iii) the bold lines represent the boundaries between the mixed and unmixed fluid. The arrows in figure 13 (*c*) are indicative of an inflow of fluid and also show the apparent streamwise rotation. This rotation appears to be caused by the streamwise stretching of flow structures immediately behind the trailing edge where there is a high velocity gradient in the flow direction.

The interaction between the two boundary layers was observed to be limited exclusively to the region of the inner wake. Occasionally, the instantaneous boundaries of mixed and unmixed flow on both sides of the plate appeared to cross, implying the cross-mixing of fluid across the centreline (figure 13*b*). Andreopoulos & Bradshaw (1980) measured this behaviour using conditional sampling of the intermittency of a temperature contaminant introduced using heating elements located on one side of their test model. They reported a 14% probability of unmixed fluid passing across the centreline. In the present study there was no consistent means of determining the passage of the unmixed fluid across the centreline. However, the visualization data illustrated that the interaction between the mixed and unmixed regions was generally confined to the interface between these regions. This interface was rarely observed to make appreciable excursions across the centreline.

For $x^+ < 15$, an unsteady stagnant region $\Delta y^+ \approx 8$ wide was observed; this region appears in figure 13 (*a*, *b*) as a bright region immediately downstream of the bubble

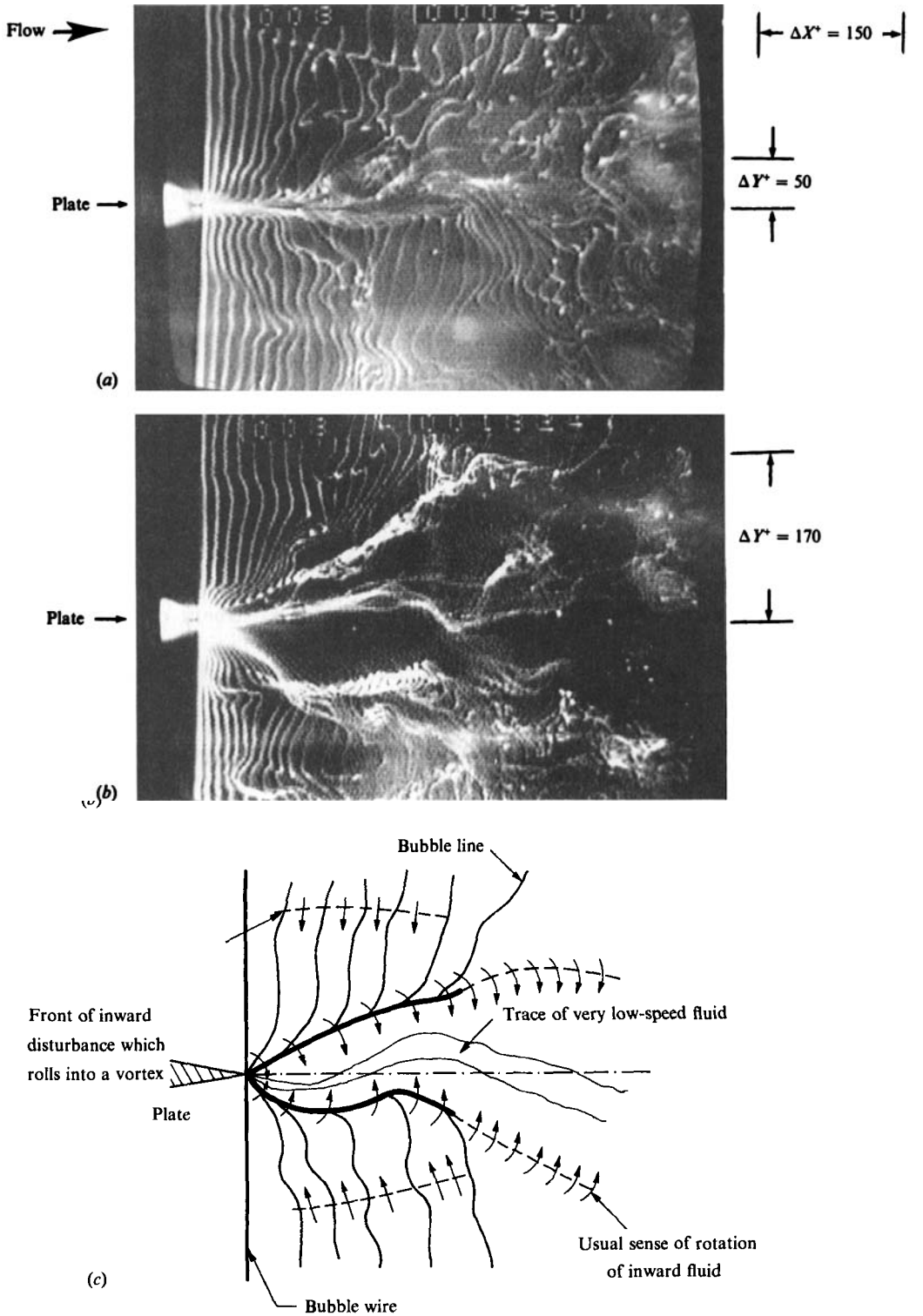

FIGURE 13. Side-view illustration of mixing process in the vicinity of the trailing edge, $x^+_{\text{wire}} = 0$, $F_{\text{HB}} = 120$ Hz. (*a*) Shear layers merging in a thin wake; (*b*) intense interaction of boundary layers involving outer-wake fluid; (*c*) schematic representation of most common mixing process.

wire. The region was quite unsteady, appearing to grow and diminish in a quasi-cyclic manner; the above dimensions represent the approximate mean stagnant bubble size. High magnification (i.e. a small field of view) was used to study the stagnant bubble. Occasionally, an unsteady vortex street with a transient frequency and scale of the order of the trailing-edge thickness was observed to shed from the plate within the $0 < x^+ < 15$ region. However, these vortices were dominated by the larger-scale streamwise vortices, and the intense streamwise stretching. Thus, these vortices would persist for no more than one shedding cycle, with their coherent activity limited to the $x^+ < 15$ region.

4.2.2. *Mixing in the region* $x^+ > 270$

Close review of side-view visual data for $x^+ > 270$ indicates the following modifications in flow characteristics in the wake as the bubble-wire is moved downstream of the trailing edge: (i) a change in the structure orientation (i.e. a slow approach towards 'homogeneity'); (ii) an increase in the vortex interaction up to $x^+ = 1500$; (iii) a decrease in the flow activity beyond $x^+ = 1500$; (iv) an increase in scales with increasing x. Additional clarification of the above developments is done with the aid of figure 14. The pictures in this figure were selected such that they represent the general types of phenomena observed at increasing distances from the trailing edge. All the pictures in figure 14 show a field of view of approximately $\Delta y^+ = 450$ by $\Delta x^+ = 650$. The emphasis in this figure is on how the apparent flow behaviour within the field of view changes with downstream distance. The schematics accompanying each picture are provided to help understand the dynamics that are illustrated in each picture. Generally, the schematics illustrate only the clearly recognizable events for each particular location. The following describes the developmental changes outlined above.

The dominant streamwise structure (figure 13), which was described earlier as a streamwise vortex associated with an inward motion, is still evident for $x^+ < 270$ (figure 14*a*, *b*). However, the flow-structure orientation is modified as x increases, yielding what appear as compact transverse vortical motions. These types of motion are illustrated by the bubble patterns labelled CC in figure 14(*c*) and BB in figure 14(*d*). By $x^+ \approx 1070$ (figure 14*e*) the streamwise orientation of the flow structures appears less dominant, probably owing to the rapid relaxation of the velocity gradient, which reduces streamwise stretching and thus the dominance of streamwise vortices. This decrease in directional dominance with distance is again apparent in figure 14(*f*) which demonstrates no clear characteristic scale nor direction. Since there is no continuous source of vorticity in the wake, the flow moves towards homogeneity as the velocity profile relaxes.

As the observed transverse vortices convect across the viewing window, a strong vortex interaction is often observed. An example of such vortex interaction is illustrated at BB in figure 14(*b*), where two counter-rotating vortices are observed to move towards each other, resulting in vortex cancellation. Another example of vortex interaction is illustrated at AC in figure 14(*d*) where a longitudinal vortex is stretched outward, resulting in what appears to be a thin elongated vortex-tube-like structure. Beyond $x^+ \approx 1500$ less vortex interaction is observed, which is due to the development of larger disturbance scales. The result is a decrease in active flow behaviour and relaxation of the velocity gradient, which reduces vortex stretching effects.

A significant aspect of hydrogen-bubble-wire visualization is the ability to reveal only the locally active flow interactions; the bubble-line visualization indicates only

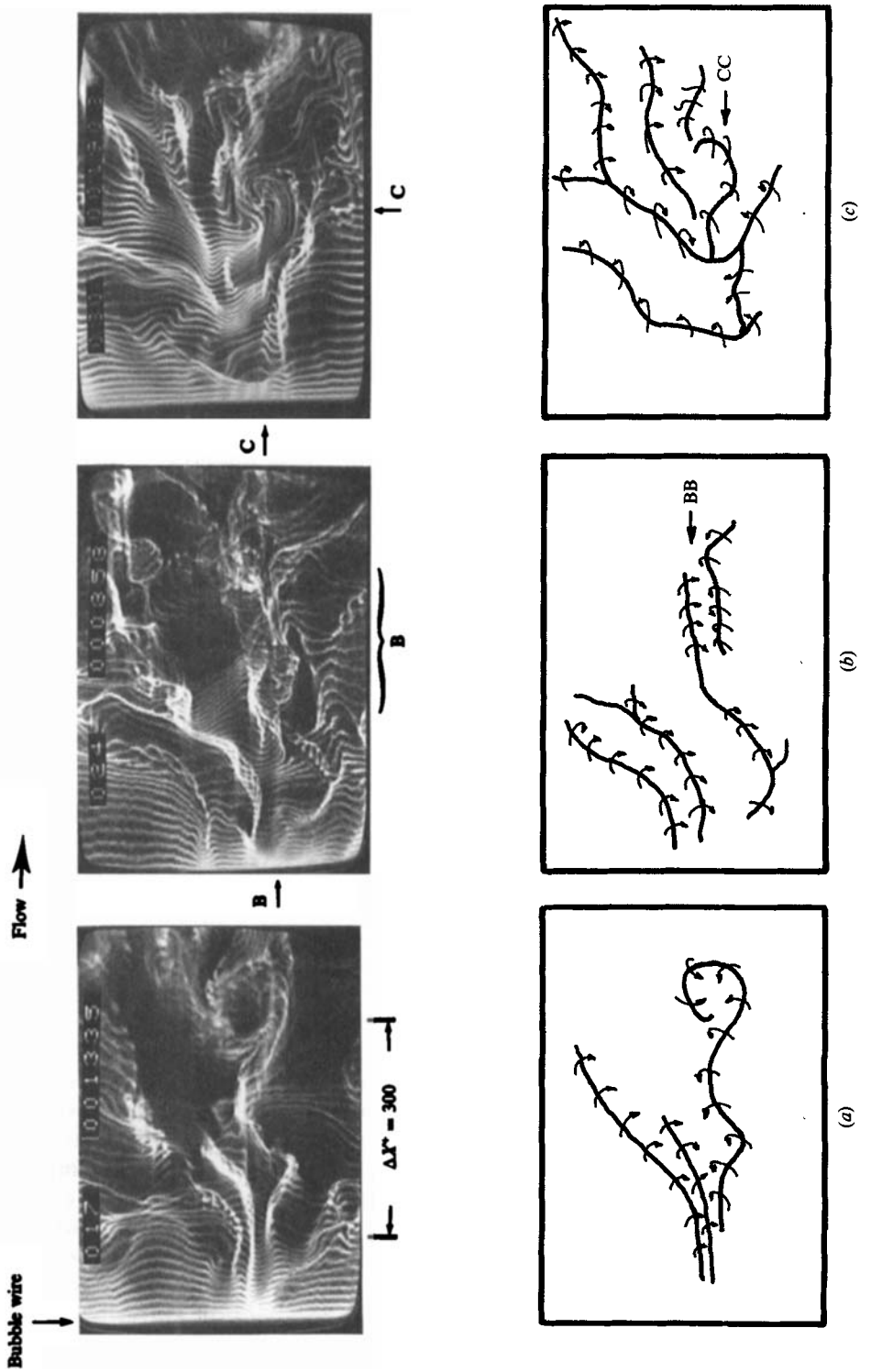

FIGURE 14 (*a–c*). For caption see facing page.

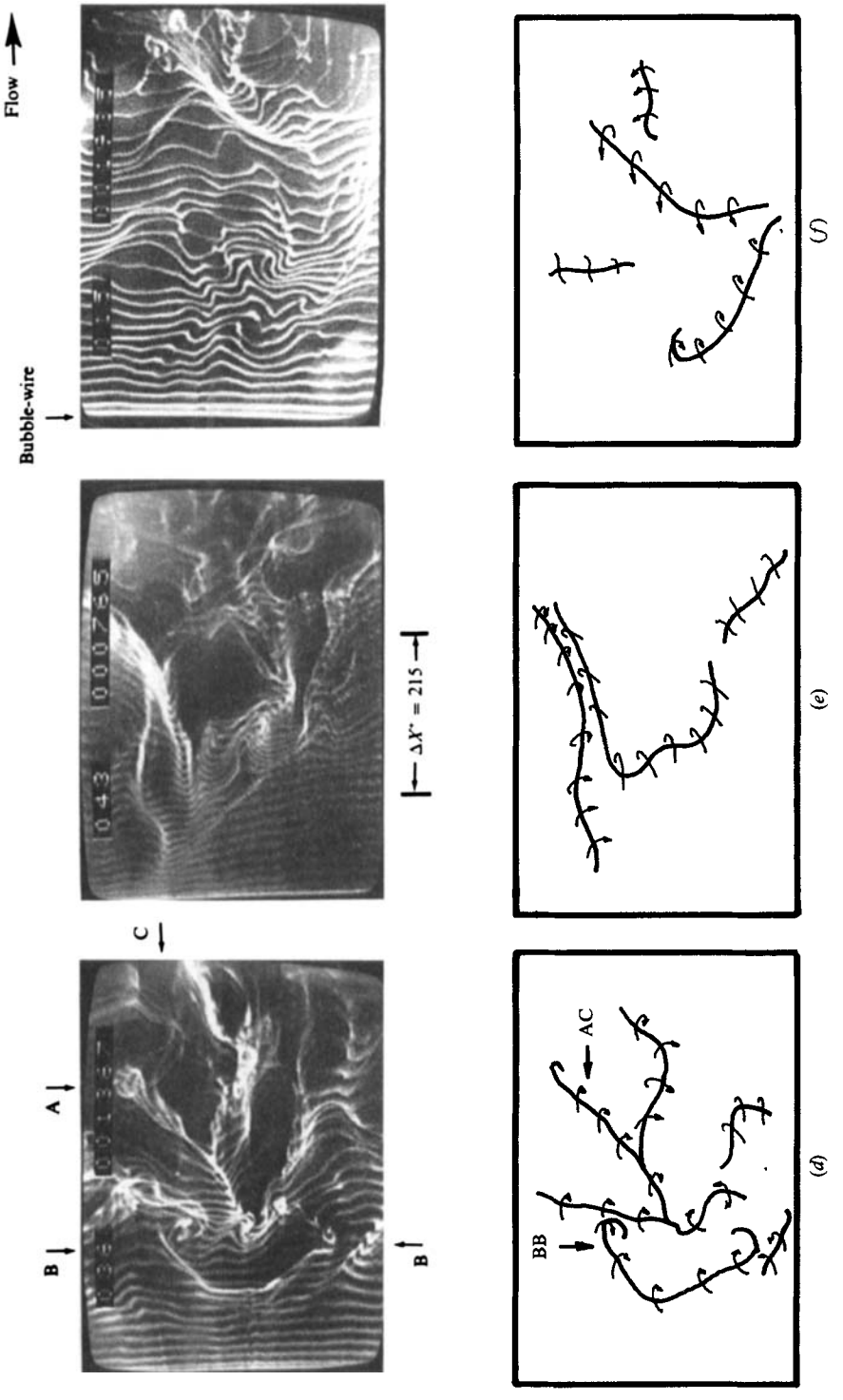

FIGURE 14. Side-view photographic sequence with schematics showing flow development with distance from the trailing edge. (*a*) $x^+ = 130$; (*b*) 270; (*c*) 540; (*d*) 800; (*e*) 1070; (*f*) 2130.

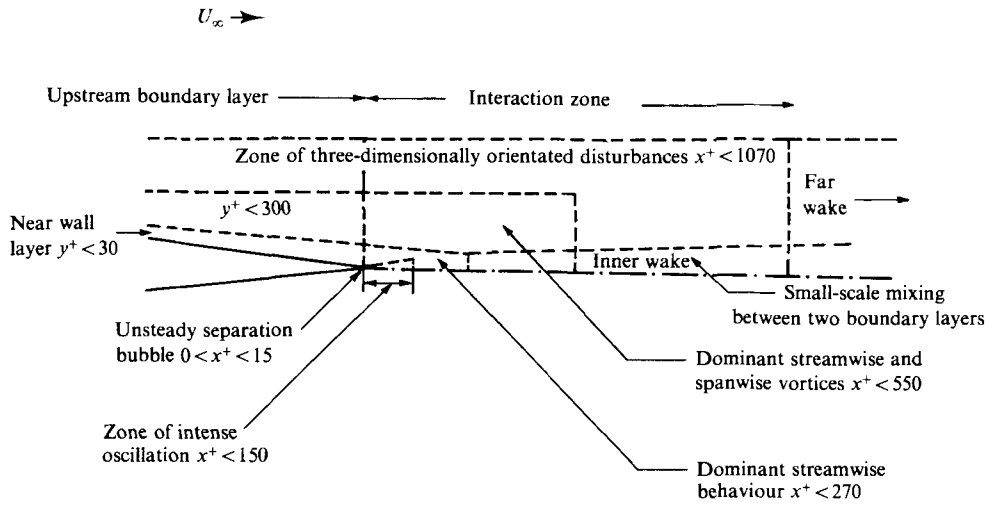

FIGURE 15. Flow structure in the vicinity of the trailing edge.

the integrated activity and motion beyond the generating bubble wire, and carries no flow history effects prior to the point of introduction. To exemplify this, note that in figure 14(*d*) the bubble lines at the left-hand side of the picture show a relatively uniform flow (at that instant). Also, a region of virtually undisturbed fluid is marked in the lower left-hand corner of the figure 14(*e*). The absence of active flow behaviour in these regions of figure 14(*d*, *e*) are examples illustrating a reduction in flow activity in comparison with the previous locations (figure 14*a–c*). Figure 14(*a–f*) clearly demonstrates that following a region of very active behaviour, $0 < x^+ < 800$, a retardation in the mixing process within the observation window occurs with increasing x.

Qualitatively it was observed that the disturbance lengthscale increases with x, similarly to the way that the scales in the boundary layer increase with y. For example, it was determined that the approximate scale of a transverse vortex at BB in figure 14(*d*) is $L^+ \approx 240$; by contrast, at $x^+ = 2200$ (figure 14*f*) a typical disturbance is almost as wide as the viewing field (i.e. $\Delta x^+ = 450$). Naturally, the stations closer to the trailing edge exhibit much smaller scales. Close to the trailing-edge tip it appears that the low-speed-streak spacing ($\bar{\lambda}^+ = 100$) is an appropriate lengthscale, as pointed out in §4.1.

4.3. *Summary of the visualization studies*

Figure 15 is an attempt to synthesize and generalize the flow behaviour observed in the voluminous visualization data. In general, three distinguishable types of behaviour were observed. Dominant streamwise structures similar to the low-speed streaks were observed, which retain their integrity to approximately $x^+ \approx 270$. As x increases, other types of flow structures, particularly transverse vortices, appear within the visualization window. For $x^+ > 800$, a streamwise dominance of the disturbances becomes less pronounced, with the flow appearing to become more and more 'homogeneous'. The interaction between the two merging boundary layers is observed to be limited to regions along and near the centreline. The zone in which the most active mixing was detected is termed the inner wake. Outside of this region the original boundary-layer structure appears to advect essentially unchanged downstream, unaware of the disappearance of the wall until the inner wake slowly

encroaches upon it. However, as distance from the trailing edge increases, the flow structure in the logarithmic region of the boundary layer becomes more involved in the mixing process, resulting in an increase in the observed disturbance lengthscales.

5. Discussion

This section discusses particular aspects of the present results that are felt to be important to future considerations of flow behaviour in the turbulent near wake of streamlined bodies. With this in mind, the observations from the hot-film-anemometry measurements and the hydrogen-bubble-wire visualization data are compared and synthesized; results from previous independent investigations are drawn upon to clarify points under consideration.

5.1. *Immediate effect of wall disappearance*, $x^+ < 270$

In the very near-wake region, immediately following termination of the trailing edge, the present visualization data clearly illustrate the immediate development of a three-layer structure. This observed behaviour is consistent with the model of Andreopoulos & Bradshaw (1980), which was developed from conditional-averaging studies employing a temperature contaminant. These layers consist of a region of intense mixing near the centreline sandwiched between the unmixed portions of the two original boundary layers. Any interaction of the mixed and unmixed regions occurs at the interface between these layers.

Following the termination of the test plate, the main contribution of the large-scale motion to the mixing is limited to a non-periodic inrush of outer fluid towards the centreline. In a hot-wire study of a similar wake-mixing process, Andreopoulos & Bradshaw (1980) observed occasional positive spikes of u' interspersed with longer regions of small negative u' at the edge of the inner wake. These positive spikes are speculated by the above authors to be the result of the inward motion of outer-region fluid. The present visualization data (§4.2.1) verify these hypothesized inrushes of fluid towards the centreline, which are detected up to $x^+ < 270$ downstream of the trailing edge. The interaction of the two opposing shear layers appears to give rise to coherent rotations oriented in the streamwise direction. However, the inrush of the flow near the sharp trailing edge does not seem to be comparable to the type of entrainment process associated with vortex shedding.

The mean- and fluctuating-velocity profile data, as well as the visualization data, indicate that the turbulent-boundary-layer properties do not change dramatically with the disappearance of the wall. This observation suggests that as flow structures originating in the boundary layer pass into the wake, they are not significantly modified for some distance downstream. The observed inflows are thus suggested to be analogous to the 'sweeps' of outer-region fluid towards the wall encountered for turbulent flow over flat plates. The mixing accompanying these inflows will promote the rapid recovery of the near-wake velocity profile in the neighbourhood of the centreline. The outward eruption of the wake interface (§4.2.1) toward and into the outer wake appears roughly similar to the turbulent 'bursting' behaviour observed in turbulent boundary layers. The negative spikes of u' detected near the edge of the inner wake by Andreopoulos & Bradshaw (1980) are also believed to be associated with the outward eruptions of fluid from regions closer to the wake centreline.

In the mixing region immediately downstream of the trailing edge, streamwise-oriented small-scale structures (for all intents and purposes appearing to be the same structure as the near-wall low-speed streaks in the boundary layer) dominate the

inner-wake mixing. Rapid growth of the wake in this region ($x^+ < 270$) was observed to be the result of interactions between these near-wall-type structures. The streamwise orientation of the flow structure appears to rapidly diminish in conjunction with the decrease in the streamwise velocity gradient in the immediate vicinity of the trailing edge for $0 < x^+ < 270$; this change in the preferred orientation appears to be clearly coupled with a sustained reduction of wake spreading and velocity-profile recovery with increasing x^+.

5.2. *Centreline and turbulent-boundary-layer profile similarity*

The near-wake flow characteristics immediately downstream of the trailing edge exhibit strong similarities to the cross-stream characteristics of a turbulent boundary layer. These similarities are best illustrated by a comparative plot (figure 16) of the centreline-velocity profile and a turbulent-boundary-layer profile (from Johansen & Smith 1986) for flow over a flat plate. The two-layer growth of the centreline velocity has prompted some researchers to analytically model the near-wake flow based on a two-layer turbulence model. A detailed discussion of these analytical solutions and their comparison with experimental data is given in Ramaprian *et al.* (1982).

The logarithmic growth of the wake centreline is well accepted. A slight discrepancy exists as to when this logarithmic growth initiates and when it terminates. As suggested by Ramaprian *et al.* (1982), an equation of the form $u^+_{\mathrm{cl}} = C_1 \ln f(x) + \text{constant}$ will adequately represent the logarithmic region.

Employing a linear form of eddy diffusivity $\epsilon = \kappa y$, Alber (1980) obtained a similarity solution for the region $10^2 < x^+ < 10^4$. Alber's equation for the wake centreline velocity, accurate to the first order takes the form of

$$u^+_{\mathrm{cl}} = 1/\kappa[\ln(g(x)) - \gamma] + B, \tag{5.1}$$

where $g(x)$ is a similarity function which arises out of the analysis, $\kappa = 0.41$, $B = 5$ and $\gamma = 0.5772157$ (Euler's constant). Equation (5.1) provides a perfect match for the Chevray & Kovasznay (1969) data for $x^+ > 500$, and it even holds for data beyond $x^+ = 10^4$ which Alber originally assumed as an upper limit. In fact, from the experiments of Pot (1979), Andreopoulos & Bradshaw (1980), and Ramaprian *et al.* (1982) it is evident that the centreline velocity behaves logarithmically well beyond $x^+ = 10^4$, although the logarithmic portion of the cross-stream profiles has become negligibly small.

Despite good agreement with data of Chevray & Kovasznay (1969), Pot (1979) and Ramaprian *et al.* (1982), Alber's wake centreline equation (5.1) does not agree particularly well with the data of Andreopoulos & Bradshaw (1980). Using a regression curve fit, the latter authors' centreline velocity can be represented by

$$u^+_{\mathrm{cl}} = 2.12 \ln x^+ - 0.711. \tag{5.2}$$

(This equation is obtained from a curve fit of the original data, which provides a better match of their experimental data than that given by the original authors.) Note that the Andreopoulos & Bradshaw data demonstrates logarithmic behaviour even up to $x^+ = 4 \times 10^4$.

A comparison of the present centreline-velocity data with (5.1) and (5.2) is shown in figure 17. As is evident from this figure, the present centreline-velocity data demonstrate higher u^+_{cl} values than (5.1) and (5.2) at the same x^+ location. This discrepancy is due to non-dimensionalization based on a lower relative friction velocity than the one used in Alber (1980) and Andreopoulos & Bradshaw (1980). Recall that for the present study a low (initial $u^* = u_{\tau 0}/u_0$ value (determined

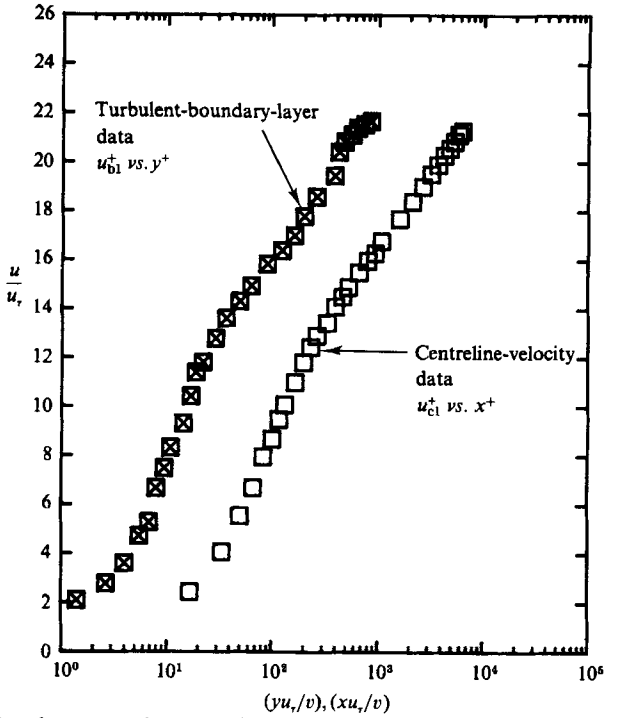

FIGURE 16. Profile of mean wake-centreline velocity *vs.* profile of turbulent flat-plate boundary layer. ⊠, Johansen & Smith (1986), $Re_\theta = 1350$; □, present, $Re_\theta = 2500$.

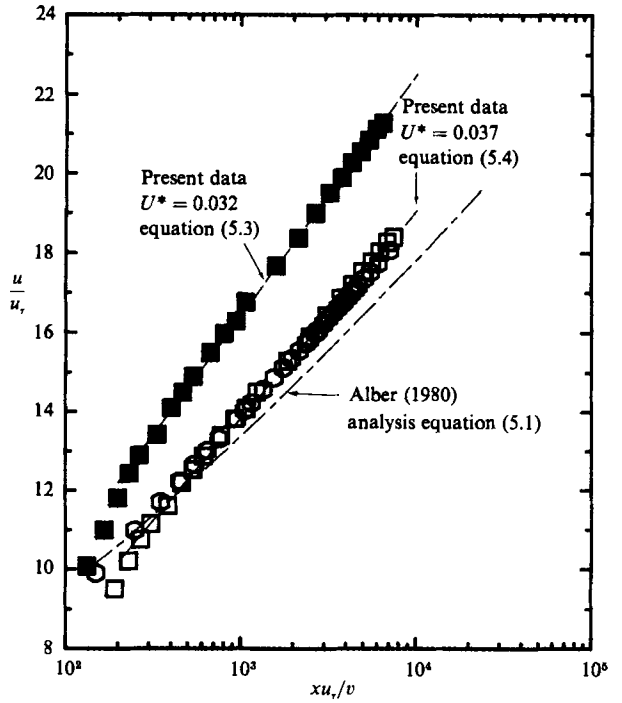

FIGURE 17. Comparison of centreline-velocity relaxation *vs.* x^+. ■, present, $u^* = 0.032$; □, present, $u^* = 0.037$; ○. Andreopoulos & Bradshaw (1980), $u^* = 0.035$ (equation (5.2)).

indirectly by a law-of-the-wall curve fit) was obtained owing to the mild pressure gradient which resulted from tapering of the trailing edge of the thick plate.

To examine the potential arbitrariness of the normalizing velocity, u_τ was varied to establish an optimal match between the Andreopoulos & Bradshaw data and the present results. A friction velocity of $u^* = 0.037$ was determined to yield a close agreement between the two data sets. The curve fits to the present centreline-velocity data using $u^* = 0.032$, and $u^* = 0.037$ are given respectively by

$$u^+_{\mathrm{cl}} = 2.635 \ln x^+ - 1.75 \quad (u^* = 0.032), \tag{5.3}$$

$$u^+_{\mathrm{cl}} = 2.279 \ln x^+ - 1.85 \quad (u^* = 0.037). \tag{5.4}$$

It thus appears that the recovery of the present wake centreline velocity occurs in a very similar manner to the results of Andreopoulos & Bradshaw. However, the need to selectively optimize u_τ to force a fit of the two data sets suggests that either: (i) the scaling of the wake development on u_τ may be somewhat arbitrary, or (ii) the determination of u_τ by a fit of the present velocity profile to the law of the wall does not provide an appropriate indication of the true wall shear stress. Since no other method for determination of u_τ is available, no firm comment can be made regarding the appropriateness of u_τ as a scaling variable for the wake. Clearly, the wake centreline velocity recovers logarithmically, but it is unclear that the appropriate scaling velocity is the u_τ determined on the test model prior to wake initiation.

Since the wake velocity does demonstrate a logarithmic recovery along the centreline, this raises the question as to whether the flow processes causing the velocity-profile development in the logarithmic region of a turbulent boundary layer are similar or related to the processes causing the relaxation behaviour of the centreline velocity in the wake. From both the visualization results (§4.1) and the hot-film data (figure 16), it appears that the growth in turbulence scales and flow structures along the wake centreline is similar to that of turbulent boundary layers. In essence, the turbulence scales along the wake centreline appear to vary with x in a manner similar to scale variations with y across boundary layers. These observed similarities suggest that an appropriate scale transformation may collapse the boundary layer and wake centreline profile to one equation.

5.3. *Transformation of y^+ to x^+*

It was empirically observed that the scale development in y for a turbulent boundary layer can be matched to the scale development in x for the wake centreline by a simple linear transformation of the form $y^+ = Kx^+$ (K is a constant). As illustrated in figure 18, applying this transformation to the well-established law-of-the-wall equation for a turbulent boundary layer,

$$u^+_{\mathrm{bl}} = 2.44 \ln y^+ + 5.9, \tag{5.5a}$$

yields

$$u^+_{\mathrm{cl}} = 2.44 \ln Kx^+ + 5.9, \tag{5.5b}$$

which closely approximates the present centreline-velocity behaviour for $x^+ > 270$.

Furthermore, the $y^+ = Kx^+$ transformation collapses the linear sublayer data of a turbulent boundary layer (from Johansen & Smith 1986) and the very near-wake centreline velocity for $x^+ \leqslant 100$. Figure 19 illustrates the comparative similarity of the centreline-velocity data with the turbulent-linear-sublayer data of Johansen & Smith (1986).

It is clear from figure 19 that the mean centreline velocity grows linearly up to

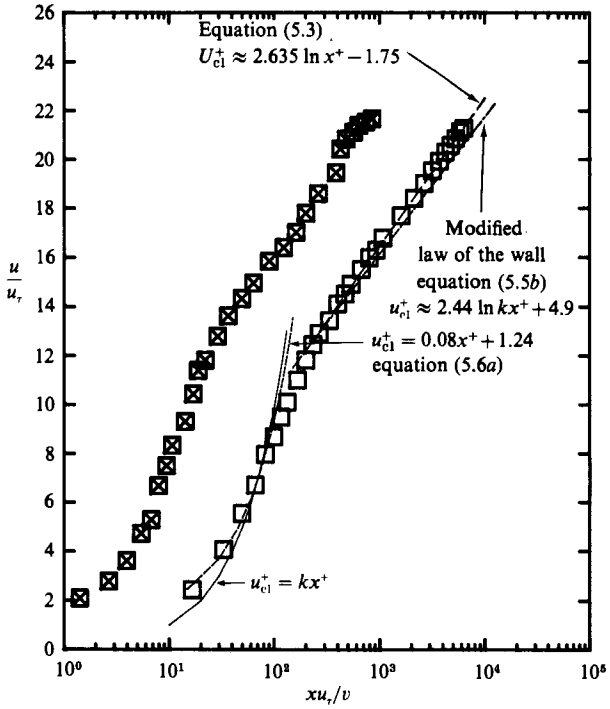

FIGURE 18. Comparison of the wake centreline-velocity profile with the law-of-the-wall and turbulent-boundary-layer profile. □, present wake flow; ⊠, Johansen & Smith (1986), turbulent boundary layer.

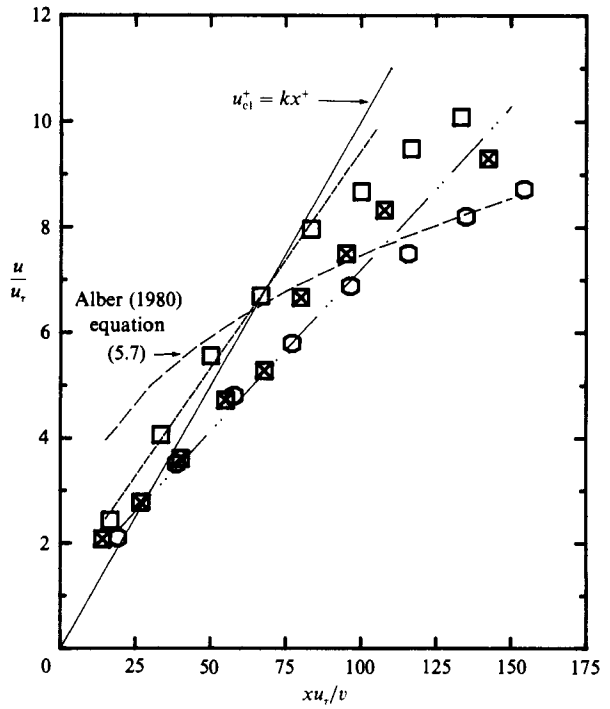

FIGURE 19. Linear velocity growth on the wake centreline for $x^+ < 100$. □, present, – – – $u_{c1}^+ = 0.082x^+ + 1.24$, $u^* = 0.032$; ○, present —··— $u_{c1}^+ = 0.061x^+ + 1.07$, $u^* = 0.037$; ⊠, boundary-layer data, Johansen & Smith (1986) plotted in transformed coordinates, $x^+ = y^+/K$.

$x^+ \leqslant 100$ in manner similar to linear sublayer growth. A linear-regression curve fit of the present data yields

$$u_{\mathrm{cl}}^+ = 0.082x^+ + 1.24. \tag{5.6a}$$

Also, recall that the bubble-wire patterns visualized in the $0 < x^+ < 130$ region (§4.1) appeared essentially the same as those for the near-wall region of a turbulent boundary layer, which suggests similar flow structure and behaviour. Analogous to arguing that $u^+ = y^+$ for $y^+ < 5$ in a turbulent boundary layer, the linear relationship of (5.6*a*) suggests that $u_{\mathrm{cl}}^+ = Kx^+$. Note that either a minimal experimental error in accurately locating the sensor relative to the trailing edge or the influence of the small separation region immediately behind the sharp taper (§4.2.1) will significantly change the origin of the linear growth region. Thus, it is not surprising to find that (5.6*a*) predicts that $u_{\mathrm{cl}}^+ \neq 0$ at $X = 0$. This suggests that (5.6*a*) should be approximated as $u_{\mathrm{cl}}^+ = Kx^+$. A parameter that can obviously affect the slope of (5.6*a*), and thus K, is u_τ. It is important to re-emphasize that u_τ is only an arbitrary normalizing parameter. Recall that a non-dimensionalized friction velocity of $u^* = 0.037$ was determined to provide a match of the logarithmic region of the present centreline-velocity data to previous investigations. Using $u^* = 0.037$ would modify (5.6*a*) to yield

$$u_{\mathrm{cl}}^+ = 0.061x^+ + 1.07. \tag{5.6b}$$

Unfortunately, there is little independent experimental information available for comparison in the region immediately downstream of the trailing edge. Furthermore, for a turbulent wake, the only analytical model known to the authors is based on the Goldstein (1930) solution for laminar centreline-velocity growth, and is suggested by Alber (1980) as

$$u_{\mathrm{cl}}^+ = 1.61(x^+)^{\frac{1}{3}}. \tag{5.7}$$

Alber indicates that this equation reasonably approximates the two data points measured on the centreline between $0 < x^+ < 300$ by Chevray & Kovasznay (1969). However, (5.7) does not appear to agree particularly well with the Chevray & Kovasznay's data and, as shown in figure 19, it also fails to represent the present measurements.

In figure 18 the centreline-velocity profile is once again plotted in comparison with a turbulent-boundary-layer profile obtained over a flat plate by Johansen & Smith (1986). In addition, (5.3), (5.5*b*) and (5.6*a*) are plotted, as well as $u_{\mathrm{cl}}^+ = Kx^+$. Note the following two points: (i) For $x^+ < 100$ the centreline velocity apparently grows linearly as $u_{\mathrm{cl}}^+ = Kx^+$. This clearly shows a parallel between growth of the linear sublayer of a turbulent boundary layer and the growth of the very near wake. (ii) For $x^+ > 270$ logarithmic behaviour of the centreline velocity is well represented by an equation of the form $u_{\mathrm{cl}}^+ = A \ln x^+ + B$. More significantly, the well-accepted law-of-the-wall equation can be easily modified to closely represent the present wake centreline-velocity data.

5.4. *Similarity in the flow development*

The centreline-velocity-data representation by (5.5*b*) indicates that the similarity of the velocity profiles shown in figures 16 and 18 is no coincidence. This in itself is a suggestion that a similar physical mechanism may govern both wake and boundary-layer growth. Therefore, it is expedient to examine why (5.5*b*) should approximate the wake data, why it is possible to match the logarithmic portions of the two experimental profiles (figure 18), and what common mechanism may be responsible for the similarity in the development of the flow profiles.

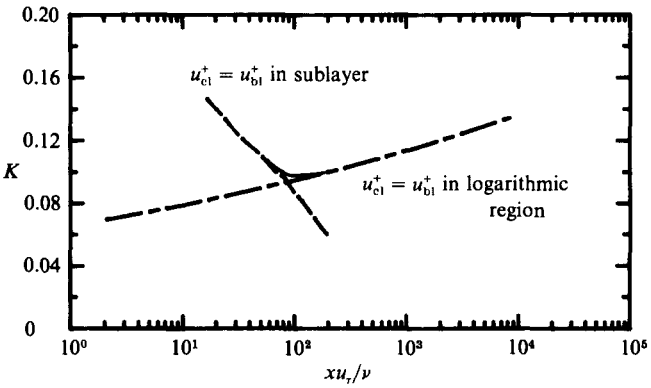

FIGURE 20. Ratio of mixing scales in the wake to those of a turbulent boundary layer, as a function of non-dimensional distance.

The remarkably similar behaviour of u^+_{cl} *vs.* x^+ suggests that the assumption of a linear turbulence-scale change with distance from the wall y within a turbulent boundary layer can be generally extrapolated to account for the scale change with distance along the wake centreline. This hypothesizes that the flow structures that grow normal to the wall in a turbulent boundary layer, and move outward relatively slowly (of the order of v), will grow in the streamwise direction in a turbulent wake as they are convected rapidly downstream (of the order of u_{cl}). Since both the boundary-layer and the centreline profiles demonstrate a logarithmic behaviour with distance from the wall or trailing edge respectively, it seems logical that a linear transformation of x^+ to the order of y^+, as demonstrated in the previous section, should collapse the behaviour of the two turbulence growth processes, and would appear to confirm the hypothesis of linear growth of turbulence scales with respective development directions.

To evaluate the assumption of a $y^+ = Kx^+$ transformation in greater detail, an examination was done of the respective values of K that provide the best fit of the centreline data of the present study with accepted turbulent-boundary-layer correlations.

In the linear growth region, a $K = y^+/x^+$ relationship is obtained by setting $u^+_{bl} = u^+_{cl}$, where $u^+ = y^+$ is the accepted empirical equation for the linear sublayer and $u^+_{cl} = Kx^+$ is assumed to govern the wake region. Thus $K = u^+_{cl}/x^+$ for the linear sublayer. For the logarithmic region, the empirical law-of-the-wall equation for a turbulent boundary layer (5.5*a*) and the equation obtained from curve fitting of the present centreline data (5.3) were used to establish K. From these two equations the ratio $K = y^+/x^+$ may be obtained by solving for the respective y^+ and x^+ where $u^+_{bl} = u^+_{cl}$.

Figure 20 illustrates the effectiveness of the $K = y^+/x^+$ transformation for both the linear and logarithmic region. Note that although K varies, it generally falls in a consistent range of 0.10 to 0.12 for the entire u^+_{cl} *vs.* x^+ range of data measured in this study. To put everything in perspective, figure 20 appears to support the suggestion that the mechanism and flow structure responsible for the velocity growth over the plate in the y-direction may be responsible for the velocity growth and mixing along the centreline as well.

Note that within a flat-plate boundary layer the mixing process is dominated by streamwise vorticity generated by the stretching/tilting of vorticity from the normal

direction by the mean-velocity gradient (i.e. essentially the $\omega_y\ \partial u/\partial y$ term in the vorticity equation), in which case the most intense mixing occurs where there is a high cross-stream velocity gradient. As distance from the wall increases, the gradient diminishes, and as a consequence the mixing process decreases.

For flow over a solid surface, $\partial u/\partial x$ is essentially negligible. In contrast, when the wall disappears the no-slip boundary condition vanishes and is replaced by a large velocity gradient in the x-direction, $\partial u/\partial x$. Analogous to the vorticity stretching/tilting effect of $\partial u/\partial y$ within the flat-plate boundary layer, the large streamwise velocity gradient along the centreline gives rise to a substantial mixing process in the x-direction which is now governed by $\omega_x\ \partial u/\partial x$. However, this rapid mixing along the wake centreline results in a rapid relaxation in u_{cl}^+ such that the stretching effect of $\partial u/\partial x$ diminishes rapidly with increasing x, essentially analogous to the rapidly diminishing stretching effect that occurs normal to the surface in a turbulent boundary layer. It would thus seem reasonable that the upstream turbulent-boundary-layer structures, which are observed to stretch and increase with y above a flat surface, will be modified and interact in a similar manner along a wake centreline with increasing x.

6. Conclusions

The present paper presents an investigation of the near wake of a thick flat plate with fully developed turbulent boundary layers and a tapered trailing edge. From the results, the following points are concluded:

(i) A slowly evolving wake initiates immediately downstream of the tapered trailing edge. The wake appears to be comprised of a three-layer structure of a 'mixed' region flanked by two 'unmixed' regions, with interactions between the two shear layers confined primarily within the 'mixed' region. The streamwise mean- and fluctuating-velocity profiles are essentially identical with previous studies of flat-plate wakes, and reveal a slowly spreading wake. The visualization data indicate that disturbance lengthscales grow with increasing x^+.

(ii) Streamwise vortex stretching appears to dominate the flow behaviour in the immediate vicinity of the wake centreline. In this region, the wake mixing process and the disturbance lengthscales grow with x^+ in a manner similar to changes in the same characteristics with y^+ within a developed turbulent boundary layer. Along the wake centreline, two distinct regions of velocity relaxation behaviour are recognized. First is a linear growth region for $x^+ \leqslant 100$ and second a logarithmic region for $x^+ \geqslant 270$. Both hot-film anemometry and flow-visualization results strongly suggest that the development of turbulence lengthscales and mixing with increasing distance from the trailing edge of a tapered flat plate occur in a similar manner to the development of those characteristics in a normal direction within a turbulent flat-plate boundary layer.

(iii) A linear transformation of the form $y^+ = Kx^+$ is shown to approximately collapse the accepted empirical correlations of $u_{\mathrm{bl}}^+ = y^+$ and $u_{\mathrm{bl}}^+ = 2.44 \ln y^+ + 4.99$ for a turbulent boundary layer and the present empirical correlations for wake centreline-velocity development to a single set of curves.

The authors wish to thank Drs J. D. A. Walker, E. A. Bogucz and R. W. Paterson for valuable discussions regarding the present work. We also gratefully acknowledge support of this research by the National Science Foundation under grant no. MEA-8016829.

REFERENCES

ALBER, I. E. 1980 Turbulent wake of a thin flat plate. *AIAA J.* **18**, 1044–1051.

ANDREOPOULOS, J. & BRADSHAW, P. 1980 Measurement of interacting turbulent shear layers in the near wake of a flat plate. *J. Fluid Mech.* **100**, 639–668.

BOGUCZ, E. A. & WALKER, J. D. A. 1988 The turbulent near wake at a sharp trailing edge. *J. Fluid Mech.* (accepted).

CHEVRAY, R. & KOVASZNAY, L. S. G. 1969 Turbulence measurements in the wake of a thin flat plate. *AIAA J.* **7**, 1641–1643.

GOLDSTEIN, S. 1930 Concerning some solutions of the boundary layer equations in hydrodynamics. *Proc. Camb. Phil. Soc.* **26**, 1–30.

HAJI-HAIDARI, A. & SMITH, C. R. 1984 Comparative study of the development of the turbulent near-wake behind a thick flat plate with both a circular and tapered trailing edge geometry. *Rep.* FM-6. Dept. of Mech. Engrg & Mech., Lehigh University, Bethlehem, PA.

JOHANSEN, J. B. & SMITH, C. R. 1968 The effect of cylindrical surface modifications on turbulent boundary layers. *AIAA J.* **24**, 1081–1087.

KLINE, S. J., REYNOLDS, W. C., SCHRAUB, F. A. & RUNSTADLER, P. W. 1967 The structure of turbulent boundary layers. *J. Fluid Mech.* **30**, 741–773.

NAKAGAWA, H. & NEZU, I. 1981 Structure of space–time correlations of bursting phenomena in an open-channel flow. *J. Fluid Mech.* **104**, 1–43.

POT, P. J. 1979 A wake boundary layer mixing experiment. In *Proc. Turbulent Shear Flow 2* (ed. L. J. S. Bradbury, F. Durst, B. E. Launder, F. W. Schmidt & J. H. Whitelaw), pp. 6.6–6.11. Springer.

RAMAPRIAN, B. R., PATEL, V. C. & SASTRY, M. S. 1982 The symmetric turbulent wake of a flat plate. *AIAA J.* **20**, 1228–1235.

SMITH, C. R. 1984 A synthesized model of the near-wall behavior in turbulent boundary layer. In *Eighth Symp. on Turbulence* (ed. G. K. Patterson & J. L. Zakin), pp. 299–325. Dept. of Chem. Engrg, University of Missouri-Rolla.

SMITH, C. R. & METZLER, S. P. 1983 The characteristics of low-speed streaks in the near-wall region of a turbulent boundary layer. *J. Fluid Mech.* **129**, 27–54.

YUHAS, L. J. & WALKER, J. D. A. 1982 An optimization technique for the development of a two-dimensional turbulent boundary layer models, *AFOSR-TR*-82-0417.